






# A Computationally Efficient Method for Updating Fuel Inputs for Wildfire Behavior Models Using Sentinel Imagery and Random Forest Classification

Amy L. DeCastro <sup>1,2,\*</sup> , Timothy W. Juliano <sup>1</sup> , Branko Kosović <sup>1</sup> , Hamed Ebrahimian <sup>3</sup>   
and Jennifer K. Balch <sup>2</sup> 

<sup>1</sup> National Center for Atmospheric Research, Boulder, CO 80307, USA; tjuliano@ucar.edu (T.W.J.); branko@ucar.edu (B.K.)

<sup>2</sup> Department of Geography, University of Colorado Boulder, Boulder, CO 80309, USA; jennifer.balch@colorado.edu

<sup>3</sup> Department of Civil and Environmental Engineering, University of Nevada Reno, Reno, NV 89557, USA; hebrahimian@unr.edu

\* Correspondence: decastro@ucar.edu

**Abstract:** Disturbance events can happen at a temporal scale much faster than wildland fire fuel data updates. When used as input for wildland fire behavior models, outdated fuel datasets can contribute to misleading forecasts, which have implications for operational firefighting, mitigation, and wildland fire research. Remote sensing and machine learning methods can provide a solution for on-demand fuel estimation. Here, we show a proof of concept using C-band synthetic aperture radar and multispectral imagery, land cover classes, and tree mortality surveys to train a random forest classifier to estimate wildland fire fuel data in the East Troublesome Fire (Colorado) domain. The algorithm classified over 80% of the test dataset correctly, and the resulting wildland fire fuel data was used to simulate the East Troublesome Fire using the coupled atmosphere—wildland fire behavior model, WRF-Fire. The simulation using the modified fuel inputs, where 43% of original fuels are replaced with fuels representing dead trees, improved the burn area forecast by 38%. This study demonstrates the need for up-to-date fuel maps available in real time to provide accurate prediction of wildland fire spread, and outlines the methodology based on high-resolution satellite observations and machine learning that can accomplish this task.

**Keywords:** wildland fire behavior model; fuel model; random forest; Sentinel; WRF-Fire



**Citation:** DeCastro, A.L.; Juliano, T.W.; Kosović, B.; Ebrahimian, H.; Balch, J.K. A Computationally Efficient Method for Updating Fuel Inputs for Wildfire Behavior Models Using Sentinel Imagery and Random Forest Classification. *Remote Sens.* **2022**, *14*, 1447. <https://doi.org/10.3390/rs14061447>

Academic Editors: Luis A. Ruiz and Andrew T. Hudak

Received: 1 February 2022

Accepted: 15 March 2022

Published: 17 March 2022

**Publisher's Note:** MDPI stays neutral with regard to jurisdictional claims in published maps and institutional affiliations.



**Copyright:** © 2022 by the authors. Licensee MDPI, Basel, Switzerland. This article is an open access article distributed under the terms and conditions of the Creative Commons Attribution (CC BY) license (<https://creativecommons.org/licenses/by/4.0/>).

## 1. Introduction

The coniferous forests of the lower Rocky Mountains are innately disposed to wild-fire [1]. Trends toward a warmer, drier climate and rapid development of the wildland–urban interface (WUI) have increased wildfire risk to human life and property in this region [2]. Additionally, fuel accumulation through historic fire suppression and the rise in fuel aridity have contributed to the risk of more severe wildfires [3]. Wildfire frequency and severity are increasing in the Western United States [4], and the largest, most severe fires have occurred since 2004 [5], motivating national discussions on risk mitigation [6].

Wildfire behavior models may be used effectively to forecast fire area, propagation direction, and other metrics essential to operational firefighting, fuel treatment, and our overall understanding of wildfire [7]. Fuel characteristics including fuel load depth, percent moisture of extinction, vegetation type, particle size, and heat content are important inputs for these models. Quantifying fuel characteristics in an accurate and timely way has been one of the main challenges of wildfire mitigation and operational management [8]. These models rely on accurate fuel data, and when data are available, the behavior models may be used reliably in pre-wildfire mitigation, and in active-fire suppression and management. However, wildfire fuels are dynamic on multiple time scales, from their response to hourly

atmospheric conditions to their response to multi-year disturbance events, such as drought or insect outbreaks. The publication of the fuel inputs commonly used for wildfire behavior modeling may occur at a frequency outpaced by these disturbance events. However, these datasets provide a robust foundation that may be mindfully adjusted to provide wildfire behavior models with updated fuel information.

LANDFIRE [9], a program that develops and publishes national geospatial datasets, hosts a suite of wildfire fuel datasets used by fire scientists and forest management teams to suppress active wildfire and plan mitigation strategies. The LANDFIRE datasets include the Scott and Burgan 40 fuel models [10], which are commonly used in wildfire behavior modeling. The fuel models are profiles of fuel characteristics including fuel bed depth, fuel load, fuel moisture of extinction, vegetation composition, and surface-area-to-volume ratio. Most fuel data sets are created by mapping (or ‘crosswalking’ in fuel modeling terminology) remotely sensed data, such as satellite reflectance values and fuel characteristics used in wildfire behavior models. To determine the appropriate fuel model for each location in a 30 m × 30 m grid across the contiguous United States (CONUS), the fuel data integrate remote sensing data, system ecology, gradient modeling, and landscape simulation. Composing fuel data sets is time consuming, and requires significant planning, resources, and funding. Understandably, the data sets are infrequently updated, which can be problematic when used as input for wildfire behavior modeling, particularly when used for operational wildfire management.

Here we present a method of refreshing fuel layer data using a case study of 2020 East Troublesome Fire in Colorado. While the most current LANDFIRE data available at the time of the fire showed the domain as healthy timber, shrub, and grassland, fire records show that the East Troublesome Fire burned through significant amounts of dead and downed timber; while this case study requires adjusting the fuel data to reflect beetle infestation and blowdown due to wind events, the same method could be applied to other scenarios, such as representing fuels before recursive burning or a shift in vegetation type. The overall goals of this work are to estimate tree mortality severity using a random forest (RF) model trained on C-band synthetic aperture radar (C-SAR) Sentinel-1 data, raw bands and vegetation indices from Sentinel-2 data, land cover vegetation classes from the United States Forest Service (USFS) Landscape Change Monitoring System (LCMS), and the Insect and Disease Detection Surveys (IDS) from the US Forest Service. We simulate a case study of the East Troublesome Fire using both the generated fuel data and the LANDFIRE data available at the time of the fire, and compare the simulations’ results with observed active fire data.

## 2. Materials and Methods

### 2.1. The East Troublesome Fire Case Study

The East Troublesome Fire was detected on 14 October 2020 northeast of Kremmling, Colorado, in the Arapaho and Roosevelt National Forests. With low humidity recovery overnight and high winds, the area was perfectly primed for fast wildfire conditions. Within the first 3 days, the fire spread to approximately 10,000 acres. Within 9 days, it had covered nearly 200,000 acres and crossed to the east side of the continental divide [11].

The East Troublesome Fire is an especially notable case study because it spread upwards of 87,000 acres in a 24 h period (21–22 October 2020). At the time of the fire, the available LANDFIRE fuel data set reflected fuel conditions from 2016. In 2016, much of the fire’s domain was classified as standing healthy timber and shrub. However, between 2016 and 2020, the timber in the fire domain experienced pine beetle outbreak, drought, and wind storms resulting in fuel conditions described as jackstraw—a tumble of very dry, downed, and standing trees [11]. Thus, we expect that a simulation of the East Troublesome Fire using the Scott and Burgan 40 fuel model layer available at the time of the fire would underestimate the burned area, as much of the fire domain was represented as healthy, standing timber and shrub in the dataset.

## 2.2. Machine Learning Approach

To update the existing fuel layer for the East Troublesome case study, we trained a RF classifier to estimate severity of tree mortality based on Sentinel-1 and Sentinel-2 imagery [12,13], the USFS-LCMS [14], and the USFS Insect and Disease Detection Survey (IDS) conducted in July 2019 [15]. These data were chosen to capture the greenness, texture, vegetation type, and level of tree mortality throughout the fire domain.

The Sentinel-1 system consists of two satellites, both in the same orbital plane, carrying C-SAR instrumentation. This research utilizes data collected in the instruments' interferometric wide swath (IW) mode, the main operational mode over land. The system has a revisit time of 5–7 days over the East Troublesome Fire location, with a 10 m spatial resolution. C-SAR data is used effectively for land cover change and classification [16]. In this research, C-SAR data is included in the set of model inputs to provide information on surface texture and to help distinguish between features such as shrubs, standing timber, and downed timber.

The Sentinel-2 system also consists of two satellites, each carrying a multispectral instrument (MSI) that sample 13 spectral bands at spatial resolutions between 10 and 60 m. The system has a revisit time over the case study location of approximately 5 days. Due to its relatively fine spatial and temporal resolution, data from this system has been used for land and maritime monitoring, as well as natural disaster management [17]. MSI data from Sentinel-2 is included to provide the RF with information on vegetation health, and to help distinguish between surface features.

The USFS-LCMS data set contains land cover change, land cover, and land use data at an annual resolution. These data are calculated by ensemble modeling techniques, using Landsat and Sentinel-2 imagery, terrain data, and LandTrendr and CCDC change detection algorithm results as inputs. The USFS-LCMS Land Cover product was used in this research to provide the model with a distinction between vegetation classes.

IDSs are conducted annually in forested public land across CONUS. Trained surveyors estimate the percentage of dead trees per acre, viewing the forest from fixed-wing planes or helicopters. The surveyors draw polygons around the affected forest areas on maps and label each polygon as one of five classes of tree mortality: 1–3% (very light), 4–10% (light), 11–29% (moderate), 30–50% (severe), and greater than 50% (very severe). The polygons are then matched with ground surveys to assign the dominant beetle species to each, as these data are primarily used to track beetle outbreaks across CONUS. The resulting data is a set of irregularly sized polygons labeled with the date of collection, the dominant beetle species, and level of tree mortality [15].

RF was chosen for this application due to its ability to handle both categorical and continuous variables and to capture complex interactions between several input variables [18]. Confusion matrices, accuracy scores, and hierarchies of feature importance may be used to confirm model accuracy and gain insight into feature dynamics. In particular, the Statistical Machine Intelligence and Learning Engine (Smile) version of RF was applied in Google Earth Engine. Google Earth Engine hosts a multi-petabyte library of geospatial data, and its code editor platform allows users to perform analyses over large amounts of data efficiently in the cloud [19].

We created cloud-free composites of Sentinel-2 imagery from July 2019 (the month of the 2019 Colorado tree mortality survey), and September 2020 (just before the East Troublesome Fire). Following Meddens, Hicke, Vierling, and Hudak [20], we then calculated the chlorophyll red-edge index, shortwave infrared to near infrared ratio, tasseled cap brightness, tasseled cap greenness, and tasseled cap wetness specific to the Sentinel-2 data. To develop training and validation data, we subset the tree mortality survey data to the fire event area (approximately 60 km × 70 km). We then generated 400 m<sup>2</sup> polygons randomly located within the tree mortality survey polygons, assigning them a label that mostly closely translates their USFS-IDS severity class to a representative Scott and Burgan fuel model (Figure 1). The very light and light tree mortality classes are labeled low load, the moderate and severe tree mortality classes are labeled moderate load, and the very severe

tree mortality class is labeled high load. Each of the three resulting classes represents a fuel model in the slash–blowdown category of the Scott and Burgan fuel models, a category used to describe timber slash or downed fuel from wind damage, while ‘crosswalking’ fuel data to fuel models is a common practice [10,21], it should be noted that it is a subjective process [22]. Effort was made to best match the USFS tree mortality classes to the fuel models based on the guidance for choosing representative fuel models provided in the original Scott and Burgan 40 fuel model publication [10]. To provide the RF model with data that captures all possible surface features within the wildfire domain, 400 m<sup>2</sup> polygons capturing healthy vegetation, bare ground, urban areas, and water comprise an additional class of other. Altogether, the RF model is provided multispectral, C-SAR, and land cover class input in sample spaces labeled either low load, moderate load, high load, or other.

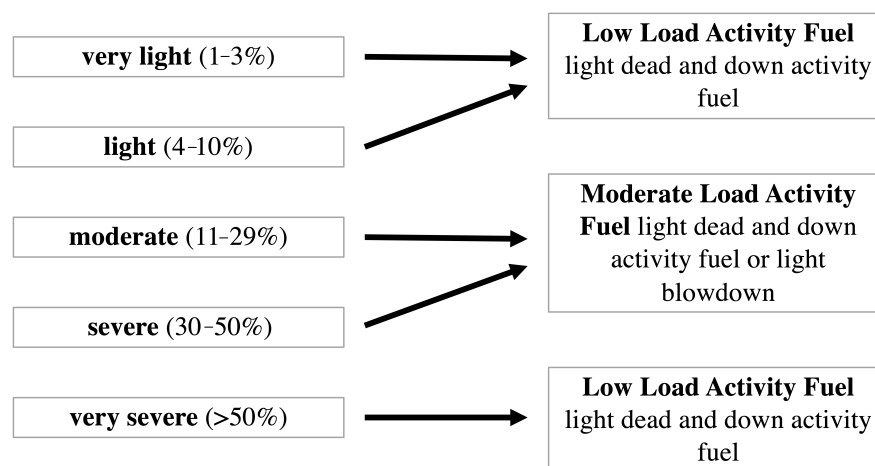


**Figure 1.** Insect and Disease Detection Survey (IDS) tree mortality classes mapped to Scott and Burgan 40 fuel models from the slash–blowdown class. Polygons from the IDS were mapped to their most representative fuel models.

The full set of polygons was split randomly into 70% for training and 30% for testing by class. The image bands, calculated indices, and land cover classes were sampled within the polygons. The RF classifier was run for the composite July 2019 image and tested for accuracy, before being applied to the September 2020 composite image. The model configuration that optimized accuracy of classifying the test dataset included 100 decision trees, 5 variables per node split, a minimum leaf population of 1, an unlimited maximum number of leaf nodes, and a bag fraction of 0.5. Once classified, the fuel layer is written in .tif format such that it may be analyzed using Python and utilized as input for a wildfire behavior model.

### 2.3. WRF-Fire

To examine the impact of the LANDFIRE fuel data on the evolution of the East Troublesome Fire, we used the weather research and forecasting (WRF) model [23] coupled to a fire behavior model based on the coupled atmosphere–wildland fire environment [24,25]. The coupled model is more commonly known as WRF-Fire [26]. In WRF-Fire, the meteorological grid is defined as in a typical WRF simulation; however, the fire grid is refined to compute fine-scale changes in the fuel properties and track the evolution of the fire perimeter via a level-set method [27,28]. Using the Rothermel [29] parametrization, the winds, fuel characteristics, and terrain slope on the fire grid determine the fire rate of spread. Once a fire is ignited in the model, the burn rate of the fuel is determined via the parametrization developed by Albini [30], which computes the amount of heat and moisture released based on the fuel properties. The released energy then feeds back to the atmosphere, such that there is full coupling between the fire and atmosphere.



Our simulations are conducted using a two-domain setup, with the outer (d01) and inner (d02) domains covering an area of approximately 220,000 km<sup>2</sup> and 32,000 km<sup>2</sup>, respectively, (Figure 2). By and large, our chosen model physics and dynamics options follow the operational WRF-Fire modeling setup, called the Colorado Fire Prediction System, developed by the National Center for Atmospheric Research (NCAR). Options relevant to this study include the following: (i) a horizontal grid cell spacing of 1000 m and 111.11 m, respectively, on the meteorological grid in d01 and d02; (ii) a horizontal grid cell spacing of 27.77 m on the fire grid in d02 (subgrid ratio of 4 compared to the meteorological grid); (iii) 44 vertical grid cells in d01 and d02; and (iv) activating the Mellor–Yamada–Nakanishi–Niino (MYNN) [31] planetary boundary layer (PBL) parametrization on d01, while d02 is run in large-eddy simulation (LES) mode. Furthermore, to determine the impact of meteorology on the wildfire evolution and bolster our results related to fuel model sensitivity, we tested two different meteorological datasets used for initial and boundary condition forcing the North American Mesoscale Forecast System (NAM) and the European Centre for Medium-Range Weather Forecasts Reanalysis v5 (ERA5).

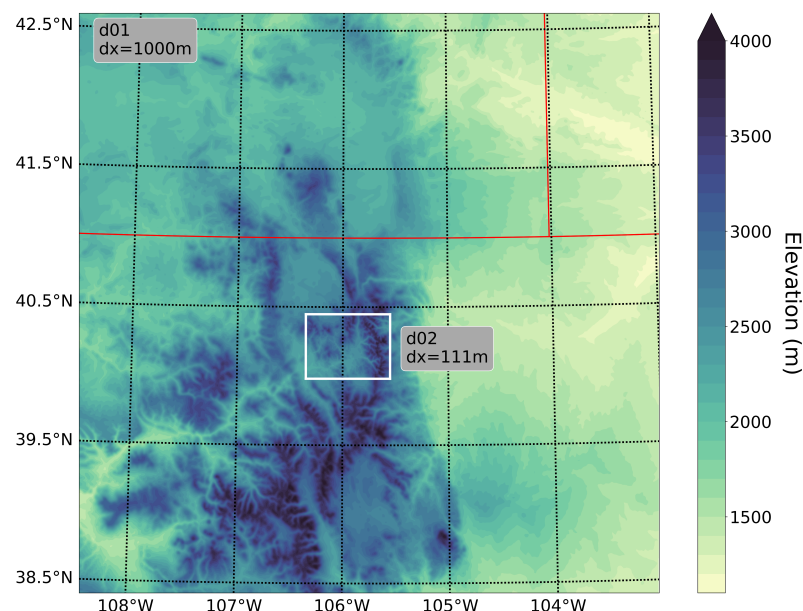


**Figure 2.** The two-domain setup used in the WRF-Fire simulations. Terrain elevation is color-contoured according to the color bar (units in m) and state outlines are represented by the solid red lines.

During the preprocessing step for WRF-Fire, the fuel categories of the Scott and Burgan 40 fuel class model are assigned to each fire grid cell. For the purposes of this study, we generate two different input files: one that contains the default Scott and Burgan 40 fuel class model and one that contains the modified Scott and Burgan 40 fuel class model following our RF results, as described above. We refer to the former simulation as Control and the latter simulation as ML (abbreviation for modified layer). The original and modified Scott and Burgan fuel model layers used in our WRF-Fire simulations are shown in Figure 3. We also utilize the 3-arc second Shuttle Radar Topography Mission (SRTM) terrain data for the fuel grid. Recent developments by NCAR allow us to apply heterogeneous fuel moisture content (FMC) values to our fire domain [32]. As an additional sensitivity test, we evaluate the impact of FMC by also conducting a simulation with constant FMC set to 9%, which is approximately equal to the domain-averaged value computed from the heterogeneous FMC data set (not shown).

In summary, we conducted a total of five simulations based on the various model sensitivities discussed above: (1) NAM Control, (2) NAM ML, (3) NAM ML + Constant FMC, (4) ERA5 Control, and (5) ERA5 ML. Each of our simulations began at 21 October

2020, 1800 UTC and ended at 22 October 2020, 1500 UTC. The fire is ignited from an active perimeter (provided by the National Inter-agency Fire Center and shown in Figure 3) measured at 22 October 2020, 0020 UTC (6 h and 20 min after the simulation start time to ensure sufficient spin-up time). We now show results from the various WRF-Fire simulations to highlight the relative impact of varying the fuel categories, meteorological forcing data set, and FMC.

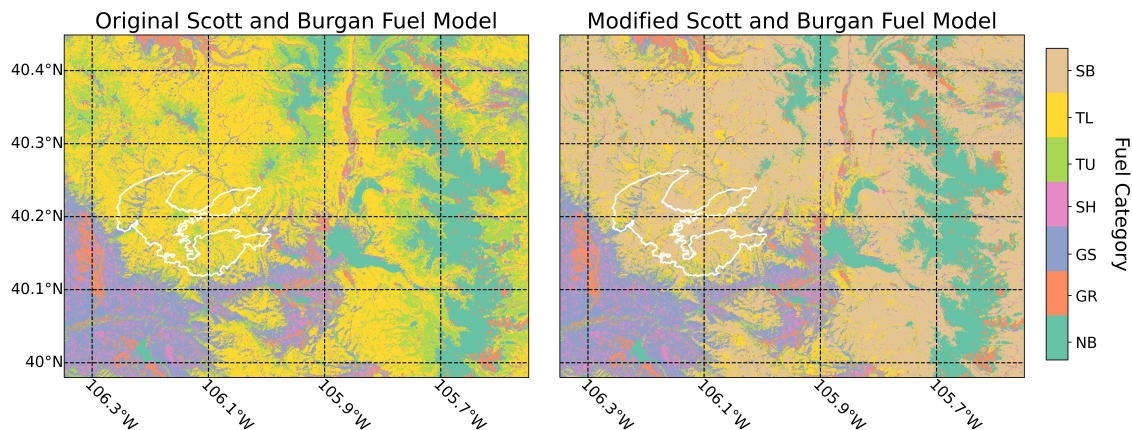


**Figure 3.** The original (left) and modified (right) Scott and Burgan fuel model layers used in the WRF-Fire simulations. The active fire perimeter used to initiate the simulations is shown in white. Fuel categories represent the fuel type of the fuel model; slash-blowdown (SB), timber litter (TL), timber-understory (TU), shrub (SH), grass-shrub (GS), grass (GR), and nonburnable (NB).

### 3. Results

The RF algorithm correctly classified over 84% of the test data in the fire domain, and performed well at separating the tree mortality classes from the other class. The RF misclassified 6.1% of the low load, <1% of the moderate load, and 8.7% of the high load classes as other. The confusion matrix for the classifier's performance on the test dataset is given in Table 1. Table 2 shows the precision (positive predictive value), recall (true positive rate), and F1 score (weighted average of precision and recall) for each class.

**Table 1.** Confusion matrix for the classifier's performance on the test dataset.

	Other	Low Load	Moderate Load	High Load
other	8505	337	257	52
low load	31	256	120	105
moderate load	8	232	457	196
high load	38	148	179	72

**Table 2.** Precision, recall, and F1-scores for the classifier's performance on the test dataset.

	Precision	Recall	F1-Score
other	0.927	0.992	0.958
low load	0.520	0.252	0.340
moderate load	0.489	0.471	0.480
high load	0.162	0.157	0.160

The fuel updating process resulted in changing a significant amount of the timber litter and timber-understory fuel classes in the original fuel model layer to slash-blowdown fuel classes in the modified fuel layer. Timber litter and timber-understory are fuel model classes in which the main fire carriers are litter such as pine needles or hardwood leaves shed from timber, and grasses, shrubs, litter, and moss, respectively. These are classes typically designated to healthy timber systems with finer fuels under the tree canopy. In

the semi-arid climate of the East Troublesome Fire case study, the wildfire rate of spread generated from these fuel models is low to moderate. In contrast, the wildfire rate of spread resulting from the slash–blowdown fuel models is moderate to high.

The WRF-Fire results from all sensitivity simulations are shown for two observed times in Figures 4 and 5, with time series of various burn area and burn rate statistics given in Figure 6. Table 3 summarizes the forecast and observed areas for each of the simulations.

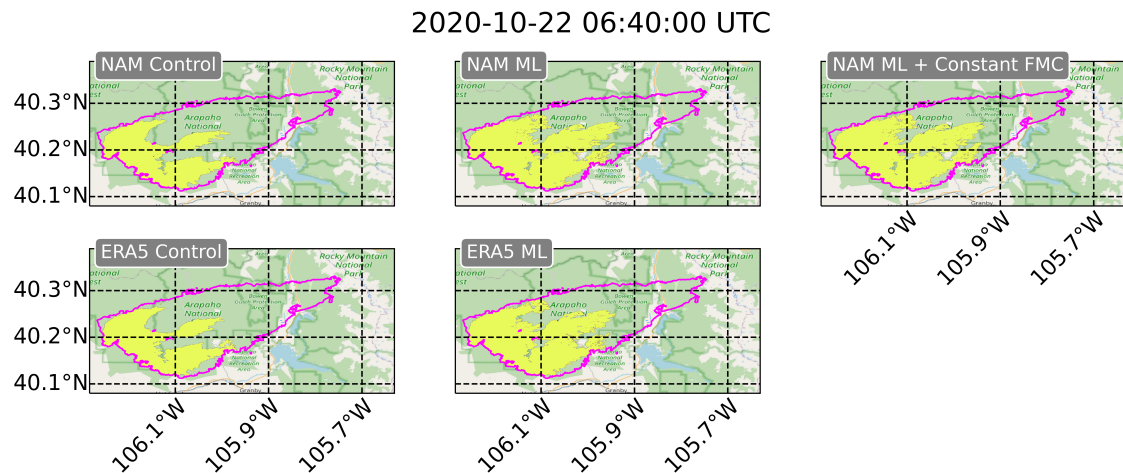


**Figure 4.** The sensitivity simulation results (solid yellow) using NAM meteorological data with the original fuel inputs, the modified fuel inputs, and the modified fuel inputs with a constant 8% fuel moisture content (labeled NAM Control, NAM ML, and NAM ML + Constant FMC, respectively), and the simulations using ERA5 with the original fuel inputs and the modified fuel inputs (labeled ERA5 Control and ERA5 ML, respectively). The observed fire perimeter (solid magenta line) was captured aerially at 06:40 UTC on 22 October 2020.

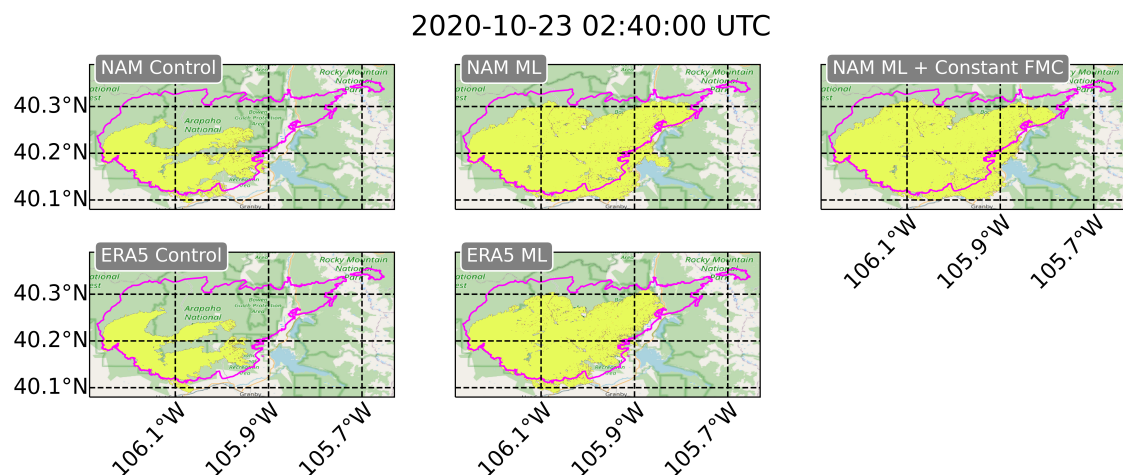


**Figure 5.** As in Figure 4, but for 02:40 UTC on 23 October 2020.

Overall, WRF-Fire underpredicts the East Troublesome Fire burn area regardless of the model setup explored in this study. Nonetheless, we find that modifying the fuel layer has the largest positive impact compared to modifying meteorological forcing data set or the FMC. Conducting simulations using the default Scott and Burgan fuel model (the fuel data that was available to incident commanders at the start time of the fire) results in a much more substantial underprediction of the burned area compared with using the updated fuel layer. As a result, the burned area prediction better matches the observed burned area, shown visually in Figures 4 and 5 and quantitatively in Figure 6 and Table 2. Additionally, our results show that forcing WRF-Fire with NAM leads to better agreement

with observations than when using ERA5, likely due to enhanced wind speeds in NAM (further explained below). For this particular case, the influence of FMC is very small compared with that of the fuel layer or meteorological forcing.

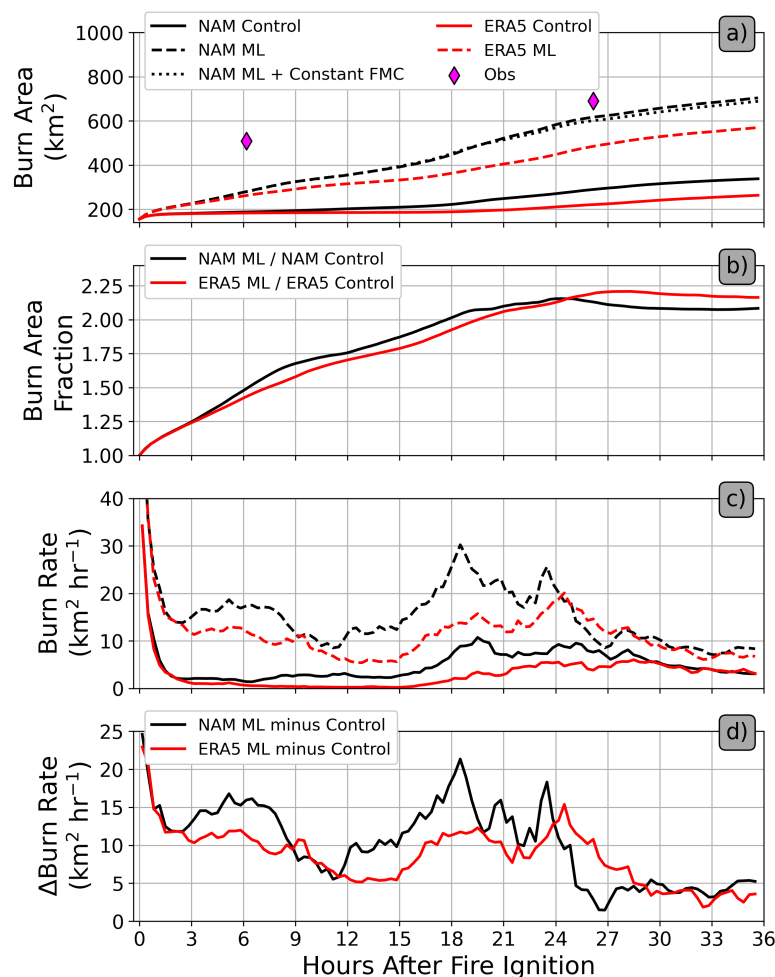


**Figure 6.** Time series of (a) burn area (km<sup>2</sup>), (b) burn area fraction (ratio of ML to Control), (c) burn rate (km<sup>2</sup> h<sup>−1</sup>), and (d) burn rate difference (ML minus Control). Model results are shown by the lines (according to the legend), while NIFC IR perimeters are shown in the magenta diamonds (labeled ‘Obs’ in the legend). The legend for panel (a) also applies to panel (c).

**Table 3.** Summary of the forecast burned area values, compared with observations occurring at the two timestamps within the simulation time frame. All forecast values in the table result from the simulations using NAM meteorological data.

Date	Simulation	Forecast Area (km <sup>2</sup> )	Observed Area (km <sup>2</sup> )	Overlap Area (km <sup>2</sup> )
10/22/20 0640 UTC	Control	188.92	508.59	179.62
	Updated Fuels	285.34	508.59	258.31
	Updated Fuels + constant FMC	284.63	508.59	259.04
10/23/20 0240 UTC	Control	293.87	689.57	272.17
	Updated Fuels	624.72	689.57	532.33
	Updated Fuels + constant FMC	608.39	689.57	531.15

A comparison of 10 m wind speeds along the fire front from the NAM Control, NAM ML, and ERA5 ML simulations are shown in Figure 7. This figure shows that the low-level



wind speeds are stronger in NAM ML compared with ERA5 ML supporting the notion that the WRF-Fire simulations with NAM initial and boundary condition forcing produce faster fire spread largely due to enhanced low-level wind speeds. In fact, the largest differences in the NAM ML and ERA5 ML lines correspond well with the largest difference in burn rate between NAM ML and ERA5 ML (Figure 6c). Furthermore, we find that the 10 m fire front wind speeds are quite similar between NAM Control and NAM ML. This result suggest that the large differences in the burned area forecasts between the Control and ML simulations may be confidently attributed to the differences between the original and modified fuel model layers and the resultant differences in fuel properties.

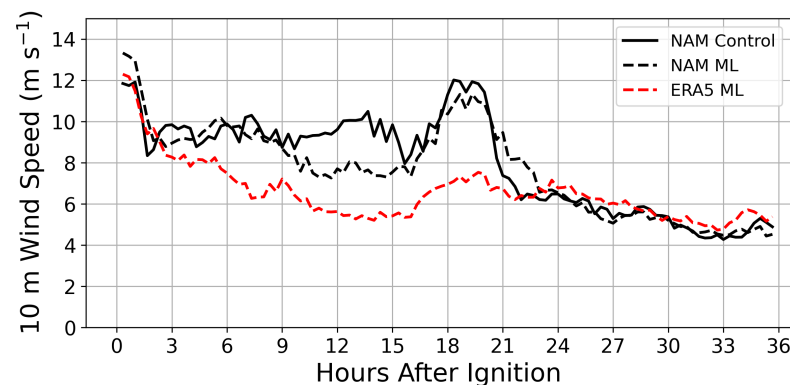


**Figure 7.** Time series of fire-front-averaged 10 m wind speed at model grid cells with active burning. We average across all horizontal grid cells where the fire rate of spread is  $>0.05 \text{ m s}^{-1}$ . Results from three select simulations are shown according to the legend.

#### 4. Discussion

Examining the confusion matrix of the RF classifier output shows that the model correctly classifies approximately 92.7% of the other category correctly, most frequently mistaking it for the low class (4.2% of the time) in the test data set. A proportion of 52% of the low class was correctly classified, and was misclassified as the moderate class 21% of the time. The RF correctly classified 48.9% of the moderate class, mistaking it for the low class 28.8% of the time. Finally, the high class was correctly classified 16.2% of the time, while mistaken for the moderate class 41.2% of the time. This analysis shows that while the model performs well at distinguishing between the other class and the slash-blowdown classes, it has not been provided enough information to excel at classifying the different severity levels. This is likely due in part to uncertainty in the training data, particularly in the tree mortality surveys as the aerial collection practices are subjective in nature [33]. Similar issues may arise in applying this method to other scenarios, which highlights the importance of including ancillary data when available and understanding the limitations of any included datasets.

The data used to train the RF classifier and to classify images were chosen with the intent of capturing information on tree mortality throughout the fire domain. In the context of a different set of known conditions, it would be necessary to choose data representative of those conditions. Regardless, the operator would need an understanding of available data and how it translates to on-the-ground conditions. Providing the RF classifier with additional information about the particular conditions just before a fire will likely improve classification accuracy when implemented mindfully.

The development and implementation of the RF in this study was performed in Google Earth Engine, which gives the Gini impurity decreases of each random forest node as a metric of feature importance. Examining the hierarchy of these values for the RF features shows that the chlorophyll red-edge index suggested by Meddens, Hicke, Vierling, and Hudak [20] is the most important feature (Figure 8). This index is particularly sensitive to chlorophyll, carotenoids, and anthocyanin production [34], which indicate vegetation senescence. There is an inevitable change in senescence simply due to the



seasonal changes between July 2019 (the time of the tree mortality surveys) and September 2020 (the time just before the East Troublesome Fire). As the chlorophyll red-edge index is important to classification, senescence may be confounded with the intended classification of tree mortality in this case. However, the C-SAR bands, which contribute information on the surface texture and were intended to help distinguish between vegetation types and standing and downed timber, were also highly important to the classification. Given the high degree of classification accuracy, this indicates that collectively the input data provided was adequate to train the RF, and that any cells classified as tree mortality due to the signature of senescence are of minimal consequence.

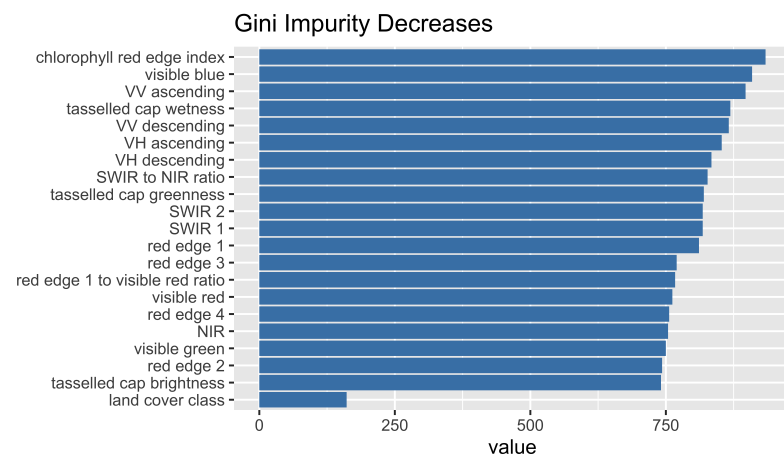


**Figure 8.** The sum of the Gini impurity decreases across all node splits for each individual random forest feature. The bars represent the importance of each feature, measured through the sum of all the Gini impurity index decreases for each feature included in the random forest classifier.

Google Earth Engine runs in the cloud and houses several relevant remote sensing data sets. Based on the methodology described in this study, it would be possible to develop an operational system that provides fuel updates in real time on an on-demand basis, and which would be available to fire behavior analysts and incident commanders. We would advise becoming familiar with the available data sets that are most relevant to the region being simulated. Moving forward more remote sensing data will become available, and may be used fruitfully for this purpose. Two additional Sentinel-1 satellites, both equipped with C-SAR instrumentation, are scheduled for launch in 2022 and 2023, and are expected to shorten the current revisit time for the system. One additional Sentinel-2 satellite is scheduled for launch in 2024, and will likewise shorten the revisit time and contribute multispectral imagery to the already established Sentinel-2 system. The fuel model data currently available provides a solid foundation for mindfully adjusting fuel layers prior to running simulations using wildfire behavior models. The incoming wealth of remote sensing data and modeling tools will only provide more opportunity for refreshing this data as needed.

## 5. Conclusions

This work presents an effective workflow for updating fuel data used in wildland fire behavior modeling. It builds on available fuel data and provides a solution to quantifying fuel characteristics in an accurate and timely manner; while the East Troublesome case study focuses on dead, downed timber due to beetle infestation and wind events, the workflow presented here may be applied to several types of disturbance events that affect wildland fire fuels, given the availability of relevant data. These methods were intentionally developed using freely available data on the analysis and modeling platform, Google Earth Engine, to make them accessible to a broad user base, including wildland fire researchers and incident commanders. We anticipate that with the increase in wildland fire activity,

research, and response, as well as the increase in availability of remotely sensed data, that these methods will aid in improving wildland fire forecasts.

**Author Contributions:** Conceptualization, A.L.D. and T.W.J.; methodology, A.L.D. and T.W.J.; software, A.L.D. and T.W.J.; validation, A.L.D., B.K. and T.W.J.; formal analysis, T.W.J.; investigation, A.L.D.; resources, B.K.; data curation, A.L.D.; writing—original draft preparation, A.L.D. and T.W.J.; writing—review and editing, B.K., H.E., and J.K.B.; visualization, A.L.D. and T.W.J.; supervision, B.K., H.E. and J.K.B.; project administration, B.K., H.E. and J.K.B.; funding acquisition, B.K. and H.E. All authors have read and agreed to the published version of the manuscript.

**Funding:** This work is supported through the National Science Foundation’s Leading Engineering for America’s Prosperity, Health, and Infrastructure (LEAP HI) program by grant number CMMI-1953333. We would also like to acknowledge high-performance computing support from Cheyenne (doi:10.5065/D6RX99HX) provided by NCAR’s Computational and Information Systems Laboratory, sponsored by the National Science Foundation.

**Data Availability Statement:** A Google Earth Engine script, which includes data acquisition, is available through the GitHub page: [https://github.com/amydecastro/wildfire\\_fuel\\_update\\_in\\_GEE](https://github.com/amydecastro/wildfire_fuel_update_in_GEE), accessed on 1 February 2022.

**Acknowledgments:** Michael J. Koontz provided valuable Google Earth Engine support as well as manuscript feedback.

**Conflicts of Interest:** The authors declare no conflict of interest. The funders had no role in the design of the study; in the collection, analyses, or interpretation of data; in the writing of the manuscript, or in the decision to publish the results.

## References

1. Jain, T.B.; Nelson, A.S.; Bright, B.C.; Byrne, J.C.; Hudak, A.T. Biophysical Settings that Influenced Plantation Survival during the 2015 Wildfires in Northern Rocky Mountain Moist Mixed-Conifer Forests. *J. For.* **2022**, *120*, 22–36. [CrossRef]
2. Radeloff, V.C.; Hesters, D.P.; Kramer, H.A.; Mockrin, M.H.; Alexandre, P.M.; Bar-Massada, A.; Stewart, S.I. Rapid growth of the US wildland-urban interface raises wildfire risk. *Proc. Natl. Acad. Sci. USA* **2018**, *115*, 3314–3319. [CrossRef] [PubMed]
3. Burke, M.; Driscoll, A.; Heft-Neal, S.; Xue, J.; Burney, J.; Wara, M. The changing risk and burden of wildfire in the United States. *Proc. Natl. Acad. Sci. USA* **2021**, *118*, 2. [CrossRef] [PubMed]
4. Parks, S.A.; Abatzoglou, J.T. Warmer and drier fire seasons contribute to increases in area burned at high severity in western US forests from 1985 to 2017. *Geophys. Res. Lett.* **2020**, *47*, e2020GL089858. [CrossRef]
5. Environmental Protection Agency, Climate Change Indicators: Wildfire. Available online: <https://www.epa.gov/climate-indicators/climate-change-indicators-wildfires> (accessed on 26 January 2022).
6. U.S. Department of Agriculture, Biden-Harris Administration Announces Over \$1 Billion in Disaster Relief Funds for Post-Wildfire and Hurricane Recovery. Available online: <https://www.usda.gov/media/press-releases/2022/01/21/biden-harris-administration-announces-over-1-billion-disaster> (accessed on 21 January 2022).
7. Cardil, A.; Rodrigues, M.; Ramirez, J.; de-Miguel, S.; Silva, C.A.; Mariani, M.; Ascoli, D. Coupled effects of climate teleconnections on drought, Santa Ana winds and wildfires in southern California. *Sci. Total Environ.* **2001**, *765*, 142788. [CrossRef] [PubMed]
8. Keane, R.E.; Burgan, R.; van Wagendonk, J. Mapping wildland fuels for fire management across multiple scales: Integrating remote sensing, GIS, and biophysical modeling. *Int. J. Wildland Fire* **2001**, *10*, 301–319. [CrossRef]
9. Rollins, M.G. LANDFIRE: A nationally consistent vegetation, wildland fire, and fuel assessment. *Int. J. Wildland Fire* **2009**, *18*, 235–249. [CrossRef]
10. Scott, J.H. *Standard Fire Behavior Fuel Models: A Comprehensive Set for Use with Rothermel’s Surface Fire Spread Model*; US Department of Agriculture, Forest Service, Rocky Mountain Research Station: Fort Collins, CO, USA, 2005.
11. Inciweb, East Troublesome Fire Information. Available online: <https://inciweb.nwcg.gov/incident/7242/> (accessed on 1 June 2021).
12. Earth Engine Data Catalog, Sentinel-1. Available online: [https://developers.google.com/earth-engine/datasets/catalog/COPERNICUS\\_S1\\_GRD?hl=en](https://developers.google.com/earth-engine/datasets/catalog/COPERNICUS_S1_GRD?hl=en) (accessed on 1 June 2021).
13. Earth Engine Data Catalog, Sentinel-2. Available online: [https://developers.google.com/earth-engine/datasets/catalog/COPERNICUS\\_S2\\_SR](https://developers.google.com/earth-engine/datasets/catalog/COPERNICUS_S2_SR) (accessed on 1 June 2021).
14. Earth Engine Data Catalog, USFS Landscape Change Monitoring System v2020.5. Available online: [https://developers.google.com/earth-engine/datasets/catalog/USFS\\_GTAC\\_LCMS\\_v2020-5?hl=en](https://developers.google.com/earth-engine/datasets/catalog/USFS_GTAC_LCMS_v2020-5?hl=en) (accessed on 1 June 2021).
15. U.S. Department of Agriculture, Forest Health. Available online: <https://www.fs.fed.us/foresthealth/applied-sciences/mapping-reporting/detection-surveys.shtml> (accessed on 10 June 2021).

16. Sentinel Online, Sentinel-1. Available online: <https://sentinels.copernicus.eu/web/sentinel/user-guides/sentinel-1-sar/applications/land-monitoring> (accessed on 13 January 2022).
17. Sentinel Online, Sentinel-2. Available online: <https://sentinels.copernicus.eu/web/sentinel/user-guides/sentinel-2-msi/applications> (accessed on 13 January 2022).
18. Breiman, L. Random forests. *Mach. Learn.* **2001**, *45*, 5–32. [[CrossRef](#)]
19. Gorelick, N.; Hancher, M.; Dixon, M.; Ilyushchenko, S.; Thau, D.; Moore, R. Google Earth Engine: Planetary-scale geospatial analysis for everyone. *Remote Sens. Environ.* **2017**, *202*, 18–27. [[CrossRef](#)]
20. Meddens, A.J.; Hicke, J.A.; Vierling, L.A.; Hudak, A.T. Evaluating methods to detect bark beetle-caused tree mortality using single-date and multi-date Landsat imagery. *Remote Sens. Environ.* **2013**, *132*, 49–58. [[CrossRef](#)]
21. Anderson, H.E. *Aids to Determining Fuel Models for Estimating Fire Behavior [Grass, Shrub, Timber, and Slash, Photographic Examples, Danger Ratings]*; USDA Forest Service General Technical Report; INT-Intermountain Forest and Range Experiment Station (USA): Ogden, UT, USA, 1982.
22. Krasnow, K.; Schoennagel, T.; Veblen, T.T. Forest fuel mapping and evaluation of LANDFIRE fuel maps in Boulder County, Colorado, USA. *For. Ecol. Manag.* **2009**, *257*, 1603–1612. [[CrossRef](#)]
23. Skamarock, W.C.; Klemp, J.B.; Dudhia, J.; Gill, D.O.; Barker, D.M.; Wang, W.; Powers, J.G. *A Description of the Advanced Research WRF Version 2*; National Center For Atmospheric Research Boulder Co Mesoscale and Microscale Meteorology Div.: Boulder, CO, USA, 2005.
24. Clark, T.L.; Coen, J.; Latham, D. Description of a coupled atmosphere–fire model. *J. Wildland Fire* **2004**, *13*, 49–63. [[CrossRef](#)]
25. Coen, J.L. *Modeling Wildland Fires: A Description of the Coupled Atmosphere-Wildland Fire Environment Model (CAWFE)*; National Center for Atmospheric Research: Boulder, CO, USA, 2013; Volume 38.
26. Coen, J.L.; Cameron, M.; Michalakes, J.; Patton, E.G.; Riggan, P.J.; Yedinak, K.M. WRF-Fire: Coupled weather–wildland fire modeling with the weather research and forecasting model. *J. Appl. Meteorol. Climatol.* **2013**, *52*, 16–38. [[CrossRef](#)]
27. Mandel, J.; Beezley, J.D.; Kochanski, A.K. Coupled atmosphere–wildland fire modeling with WRF 3.3 and SFIRE 2011. *Geosci. Model. Dev.* **2011**, *4*, 591–610. [[CrossRef](#)]
28. Muñoz-Esparza, D.; Kosović, B.; Jiménez, P.A.; Coen, J.L. An accurate fire-spread algorithm in the Weather Research and Forecasting model using the level-set method. *J. Adv. Model. Earth Syst.* **2018**, *10*, 908–926. [[CrossRef](#)]
29. Rothermel, R.C. *A Mathematical Model for Predicting Fire Spread in Wildland Fuels*; Intermountain Forest Range Experiment Station, Forest Service, US Department of Agriculture: Ogden, UT, USA, 1972; Volume 115, pp. 5–32.
30. Albini, F.A.; Brown, J.K.; Reinhardt, E.D.; Ottmar, R.D. Calibration of a large fuel burn-out model. *Int. J. Wildland Fire* **1995**, *5*, 173–192. [[CrossRef](#)]
31. Nakanishi, M.; Niino, H. An improved Mellor–Yamada level-3 model with condensation physics: Its design and verification. *Bound.-Layer Meteorol.* **2004**, *112*, 1–31. [[CrossRef](#)]
32. McCandless, T.C.; Kosovic, B.; Petzke, W. Enhancing wildfire spread modeling by building a gridded fuel moisture content product with machine learning. *Mach. Learn. Sci. Technol.* **2020**, *1*, 305010. [[CrossRef](#)]
33. Coleman, T.W.; Graves, A.D.; Heath, Z.; Flowers, R.W.; Hanavan, R.P.; Cluck, D.R.; Ryerson, D. Accuracy of aerial detection surveys for mapping insect and disease disturbances in the United States. *For. Ecol. Manag.* **2018**, *430*, 321–336. [[CrossRef](#)]
34. Gitelson, A.A.; Keydan, G.P.; Merzlyak, M.N. Three-band model for noninvasive estimation of chlorophyll, carotenoids, and anthocyanin contents in higher plant leaves. *Geophys. Res. Lett.* **2006**, *33*. [[CrossRef](#)]